Roles of the Species-Specific Subdomain and the N-Terminal Peptide of *Toxoplasma gondii* Ferredoxin-NADP$^+$ Reductase in Ferredoxin Binding†

Vittorio Pandini,‡ Gianluca Caprini,‡ Gabriella Tedeschi,§ Frank Seeber,|| Giuliana Zanetti,‡ and Alessandro Aliverti*,‡

Dipartimento di Scienze Biomolecolari e Biotecnologie, Università degli Studi di Milano, via Celoria 26, 20133 Milano, Italy, Dipartimento di Patologia Animale, Igiene e Sanità Pubblica Veterinaria, Università degli Studi di Milano, Via Celoria 10, 20133 Milano, Italy, and FB Biologie/Parasitologie, Philipps-Universität Marburg, Karl-von-Frisch-Strasse, 35032 Marburg, Germany

Received November 14, 2005; Revised Manuscript Received January 26, 2006

ABSTRACT: The plant-type ferredoxin/ferredoxin-NADP$^+$ reductase (Fd/FNR) redox system found in parasites of the phylum Apicomplexa has been proposed as a target for novel drugs used against life-threatening diseases such as malaria and toxoplasmosis. Like many proteins from these protists, apicomplexan FNRs are characterized by the presence of unique peptide insertions of variable length and yet unknown function. Since three-dimensional data are not available for any of the parasite FNRs, we used limited proteolysis to carry out an extensive study of the conformation of *Toxoplasma gondii* FNR. This led to identification of 11 peptide bonds susceptible to the action of four different proteases. Cleavage sites are clustered in four regions of the enzyme, which include two of its three species-specific insertions. Such regions are thus predicted to form flexible surface loops. The protein substrate Fd protected FNR against cleavage both at its N-terminal peptide and at its largest sequence insertion (28 residues). Deletion by protein engineering of the species-specific subdomain containing the latter insertion resulted in an enzyme form that, although catalytically active, displayed a 10-fold decreased affinity for Fd. In contrast, removal of the first 15 residues of the enzyme unexpectedly enhanced its interaction with Fd. Thus, two flexible polypeptide regions of *T. gondii* FNR are involved in Fd interaction but have opposite roles in modulating the binding affinity for the protein ligand. In this respect, *T. gondii* FNR differs from plant FNRs, where the N-terminal peptide contributes to the stabilization of their complex with Fd.

With few exceptions, all apicomplexan species possess a phylum-specific organelle, called an apicoplast (*1*−*3*), probably originated by a secondary endosymbiotic event between their common ancestor and a red alga (*4*). This plastid-like organelle was shown to play an essential role in the biosynthetic metabolism of these protists and is required for their long-term survival (*5*). This observation, together with the fact that plastid-like structures are not present in vertebrate cells, has recently drawn attention to the apicoplast as a possible target for both old and new drugs used against diseases caused by Apicomplexa, like malaria, toxoplasmosis, and coccidiosis (*6*, *7*). We previously demonstrated that the apicoplast of *Toxoplasma gondii* and *Plasmodium falciparum* contains a plant-type ferredoxin-NADP$^+$ reductase (FNR)[1] and ferredoxin (Fd) (*8*) and that the two proteins were able to interact in vitro and in vivo to exchange electrons with high efficiency (*9*). The conclusion from these studies was that in the apicoplast FNR could play the same role its plant counterpart plays in nonphotosynthetic plastids, i.e., the transport of electrons from NADPH to Fd for the needs of Fd-dependent reductive pathways in the organelle. Recently, it was shown that a reconstituted in vitro electron transport system based on recombinant *P. falciparum* FNR and Fd is effective in providing electrons to (*E*)-4-hydroxy-3-methyl-but-2-enyl diphosphate reductase (LytB) (*10*). This enzyme synthesizes activated isoprene units as the last step of the non-mevalonate isoprenoid biosynthesis, an apicoplast-localized pathway known to be essential for the parasite (*11*). Apicoplast FNR and Fd could thus be excellent targets for novel drugs active against apicomplexan parasites (*12*). In this respect, it is important to structurally characterize the FNR−Fd complex and to identify those surfaces involved in the intermolecular interaction. While the atomic coordinates of *P. falciparum* Fd have been recently deposited (PDB entry 1IUE, unpublished), the three-dimensional structure of any apicomplexan FNRs is still lacking, despite intensive efforts by us to crystallize *T. gondii* FNR (TgFNR). Consequently, information about the native conformation of apicomplexan FNRs has been deduced only from sequence comparisons and homology modeling (*13*, *14*). The similarity of the apicomplexan FNRs with their plant homologues extends over the entire sequence and is maximal with the root isoform (up to 51% identical) (*9*). Residues of the apicomplexan proteins poorly conserved in plant FNRs are

† This work was supported by a grant from Ministero dell'Istruzione, dell'Università e della Ricerca of Italy (Prin 2004), to G.Z.

* To whom correspondence should be addressed. Telephone: +39 02 50314897. Fax: +39 02 14895. E-mail: alessandro.aliverti@unimi.it.

‡ Dipartimento di Scienze Biomolecolari e Biotechnologie.

§ Dipartimento di Patologia Animale, Igiene e Sanità Pubblica Veterinaria.

|| Philipps-Universität Marburg.

[1] Abbreviations: FNR, ferredoxin-NADP$^+$ reductase; Fd, ferredoxin; TgFNR, *T. gondii* FNR; TgFd, *T. gondii* Fd; INT, iodonitrotetrazolium violet; MALDI-TOF, matrix-assisted laser desorption ionization time-of-flight; PMSF, phenylmethanesulfonyl fluoride.

10.1021/bi052326w CCC: $33.50
Published on Web 02/24/2006

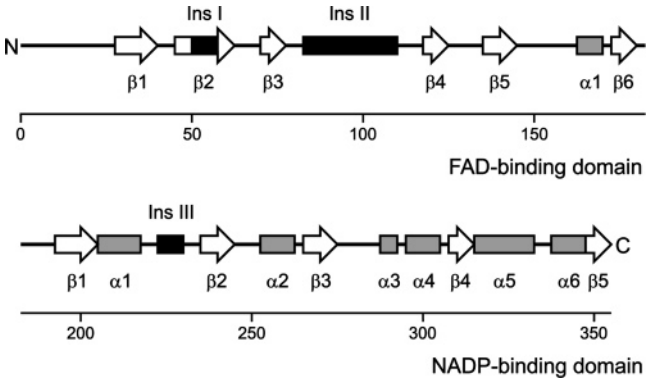

FIGURE 1: Homology-based prediction of the secondary structure and domain organization of wild-type TgFNR. The displayed model was deduced by the alignment of the TgFNR sequence with that of corn root FNR and was confirmed by the alignment with other plant-type FNRs with known three-dimensional structures. The protein sequence has been split into two parts corresponding to its two structural domains. The sequence numbering is reported below the model. The three major insertions of TgFNR (of 8, 28, and 7 residues, respectively, as compared to the corn root FNR sequence) are shown as black boxes. β strands and α helices are represented by white arrows and gray boxes, respectively.

clustered within few small segments of their sequence, namely, the N-terminal region and various insertions, whose positions are well conserved within apicomplexan FNRs (*8*). Long peptide insertions are a common feature of many apicomplexan proteins, but their functional significance is unclear (*13*−*16*). TgFNR contains three major insertions (*13*), as schematically shown in Figure 1. Two of them (insertions I and III) are expected to be far from the active site in the folded protein on the basis of the deduced position of their insertion points in the three-dimensional structure of plant FNRs. On the other hand, the much larger insertion II (28 residues with respect to maize root FNR) is located between two adjacent β strands of the β barrel forming the FAD-binding domain, at a site very close to the isoalloxazine ring of FAD. The topologically equivalent region in plant and cyanobacterial FNRs folds as a surface loop (residues 78−89 in maize root FNR) involved in Fd binding (*19*−*21*). Insertion II of TgFNR is expected to greatly enlarge such a loop, forming a subdomain (residues 81−118) within the N-terminal domain of the protein (*13*). This polypeptide region has been shown previously to be immunogenic and was therefore assumed to be solvent-exposed (*13*). In this report, we used a combination of limited proteolysis and protein engineering to gain insight in the molecular surface region of TgFNR involved in Fd binding. Our data highlight some important differences between *T. gondii* and plant photosynthetic FNRs as far as their interaction with the respective protein substrate is concerned.

MATERIALS AND METHODS

Materials. *Pfu* DNA polymerase used in PCR amplifications was from Stratagene. Chromatographic columns and media were obtained from Amersham Biosciences. Trypsin (TPCK-treated) and thermolysin were purchased from Sigma-Aldrich. Endoproteinase Glu-C (also known as SV8 protease) and endoproteinase Asp-N were from Roche. Commercial horse heart cytochrome *c* (Sigma-Aldrich) was further purified by cation-exchange chromatography on SP-Sepharose before being used in activity assays. All other chemicals were analytical or higher grade and were purchased from Sigma-Aldrich.

Plasmid Construction. The DNA sequence encoding the mature form of TgFNR starting at residue 143 of the precursor protein (*8*) was amplified by PCR using pQE-L/TgFNR (*9*) as a template. The sense primer (5′-CCGAGCTCATCGAGGGTAGGGCGACCCCGACCGACCAAAC-3′) included a *Sac*I site (underlined) and the four codons of the Ile-Glu-Gly-Arg tetrapeptide recognized by factor Xa, while the antisense primer (5′-CGCAAGCTTACTAGTACACCTCAACGTGTGCCATC-3′) contained a *Hin*dIII site (underlined). After digestion with *Sac*I and *Hin*dIII, the fragment was inserted between the same sites of the pET28b expression vector (Novagen), yielding the pET-A/TgFNR plasmid. The pET-A/TgFNRΔ(81-118)G_3 plasmid, expressing a TgFNR form carrying an internal 38-amino acid residue deletion, was obtained from pET-A/TgFNR by site-directed mutagenesis, using the ExSite PCR-Based Site Directed Mutagenesis Kit (Stratagene). The oligonucleotides 5′-GGTGGCGGTTTGCTTCCGCGGATATACAGC-3′ and 5′-TTGTGGCATGATGCCTATCCC-3′ were used as the sense and antisense primer, respectively. To improve the low efficiency experienced following the protocol provided by the kit manufacturer, an additional step was introduced, consisting of the purification by agarose gel electrophoresis of the linear DNA generated by PCR before its recircularization by ligation. The DNA sequence encoding mature TgFd was amplified by PCR from pS1TgFd (*9*) using the oligonucleotides 5′-CATGCCATGGCTCTCTTTCACCGGATAAAACTGC-3′ (sense primer) and 5′-CGGAATTCTCACTCGTCTCCGCCTTCAC-3′ (antisense primer), which introduced a *Nco*I restriction site and a *Eco*RI restriction site at the 5′-end and 3′-end of the coding sequence, respectively. The fragment was cloned between the same sites of pET28b, yielding the pET-TgFd plasmid. The insert of the three expression plasmids was entirely sequenced to exclude the presence of artifacts.

Overproduction and Purification of TgFNR Forms and TgFd. TgFNR, TgFNRΔ(81−118)G_3, and TgFd were overproduced in Rosetta(DE3) *Escherichia coli* cells (Novagen), harboring the pET-A/TgFNR, pET-A/TgFNRΔ(81−118)G_3, and pET-TgFd plasmids, respectively. Cells were grown in 2×YT medium supplemented with 30 mg/L kanamycin and 20 mg/L chloramphenicol and induced in the mid-log phase with 0.1 mM IPTG for 2−3 h. The growth temperature was 37 °C for TgFd overproduction and 25 °C for the synthesis of the TgFNR forms. After being harvested by centrifugation, cells were disrupted by sonication to yield the cell-free extracts. All chromatographic separations were carried out on an automated Äkta FPLC apparatus (Amersham Biosciences). For the purification of the TgFNR forms, the clarified cell-free extract was loaded on a Ni−Sepharose high-performance column, equilibrated with 50 mM NaP_i (pH 8.0) containing 500 mM NaCl, 5 mM imidazole, 10% glycerol, 1 mM β-mercaptoethanol, and 1 mM PMSF. After extensive washing with the same solution containing 20 mM imidazole, the enzyme was eluted by increasing the concentration of imidazole to 500 mM by a linear gradient in 2 column volumes. The fraction containing the flavoprotein was brought to 25% saturation of ammonium sulfate and loaded on a phenyl-Sepharose high-performance column,

equilibrated in 50 mM Tris-HCl (pH 7.4) containing a 25% saturation of ammonium sulfate, 1 mM EDTA, and 1 mM DTT. After the column had been washed, TgFNR was eluted with a decreasing ammonium sulfate gradient to 0% in 2 protein solution volumes. After the column had been desalted by gel filtration on a HiPrep desalting column, the His tag was removed from the enzyme by incubation with factor Xa at a 1:2000 protease:substrate (w/w) ratio for 14 h at 15 °C in 50 mM Tris-HCl (pH 8.0) containing 10% glycerol, 100 mM NaCl, and 7 mM $CaCl_2$. The digested protein was then desalted as before and loaded on a SP-Sepharose high-performance column equilibrated in 20 mM Na-HEPES (pH 7.0) containing 10% glycerol and 1 mM DTT. Elution was achieved by a linear gradient of NaCl in the same buffer from 0 to 1 M in 4 column volumes. After concentration by ultrafiltration, the TgFNR forms were stored at −80 °C in 50 mM Tris-HCl (pH 7.4) containing 10% glycerol and 1 mM DTT. TgFd was purified as previously described for recombinant spinach leaf FdI (*22*). Purified TgFd was stored at −80 °C in 150 mM Tris-HCl (pH 7.4) under nitrogen.

Limited Proteolysis. TgFNR forms (20 μM) were incubated at 25 °C in the presence of different concentrations (ranging from 0.5 to 10% in weight) of various proteases in 50 mM Na-HEPES (pH 7.5). When present, NADP$^+$ and TgFd were at concentrations of 1 mM and 120 μM, respectively. At time intervals, aliquots of the reaction mixtures were withdrawn and the proteolytic reaction was stopped before subsequent analysis. Before analysis by SDS−PAGE on analytical 12% polyacrylamide gels, samples were treated at 100 °C for 5 min with SDS and β-mercaptoethanol. Molecular mass markers were either the Dalton Mark VII-L (66, 45, 36, 29, 24, 20.1, and 14.4 kDa) or the SDS-6H (116, 97.5, 66, 45, and 29 kDa) from Sigma-Aldrich. Images of the SDS−PAGE Coomassie-stained gels were acquired by the Kodak EDAS 290 system and analyzed using ImageJ (National Institutes of Health, Bethesda, MD). To study the effect of the proteolytic degradation on the catalytic activity of TgFNR, NADPH-$K_3Fe(CN)_6$ reductase and NADPH-cytochrome *c* reductase activities were assayed on aliquots withdrawn from the reaction mixtures that were treated with a 10-fold excess in weight of bovine pancreas trypsin inhibitor in the case of trypsin, 10 mM EDTA in the case of thermolysin, or a 10-fold concentration of the "complete" (Roche) inhibitor cocktail in the case of Glu-C and Asp-N proteases.

Peptide Identification. For the determination of their N-terminal sequence, the polypeptides generated by limited proteolysis were separated by SDS−PAGE on preparative 12% polyacrylamide gels and transferred on Immobilon-P^{SQ} membranes (Millipore). Automated sequence analysis was performed on a pulsed-liquid sequencer equipped with a PTH analyzer (Procise model 491, Applied Biosystems, Foster City, CA). Matrix-assisted laser desorption ionization time-of-flight (MALDI-TOF) mass spectrometric analyses were performed on the peptide mixture by using a Bruker Daltonics Reflex IV instrument (Bruker Daltonics, Milan, Italy) equipped with a nitrogen laser (337 nm), and operated in linear mode with a matrix of sinapinic acid in 0.1% TFA and CH_3CN (2:1). External standards were used for calibration (Bruker protein calibration standard). Each spectrum was accumulated for at least 30 laser shots.

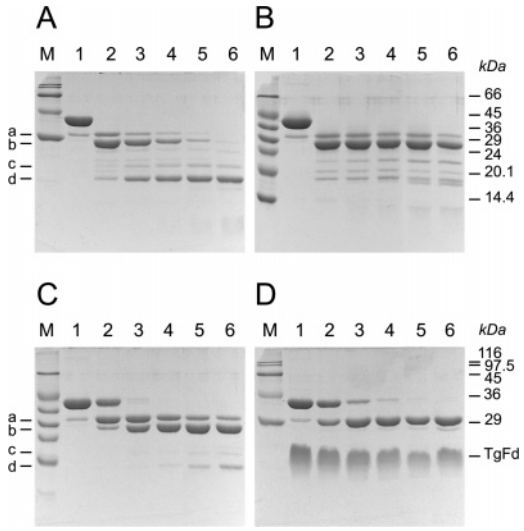

FIGURE 2: SDS−PAGE patterns of degradation of TgFNR by trypsin in the absence and presence of NADP$^+$ or TgFd. Lane M contained molecular mass markers. Lane 1 contained mixtures before trypsin addition. Lanes 2−6 contained mixtures after incubation for 1, 5, 10, 20, and 40 min, respectively. Trypsin was present in a mass ratio relative to TgFNR as specified below. (A) Incubation with 10% trypsin in the absence of TgFNR ligands. (B) Incubation with 10% trypsin in the presence of NADP$^+$ at a saturating concentration. (C) Incubation with 0.5% trypsin in the absence of TgFNR ligands. (D) Incubation with 0.5% trypsin in the presence of TgFd at a saturating concentration.

Activity Assays. NADPH-cytocrome *c* (in the presence of TgFd), NADPH-$K_3Fe(CN)_6$, and NADPH-INT reductase activities were measured as previously described (*9*, *23*).

Chromatographic Analyses. Immobilization of TgFd on Sepharose resin and analysis of the interaction of the TgFNR forms by affinity chromatography were performed as previously described (*9*, *14*). Gel filtration experiments were carried out using an Äkta FPLC apparatus equipped with a Superdex 75 HR 10/30 column in 20 mM Tris-HCl (pH 7.4) containing 200 mM NaCl and 1 mM DTT. The calibration curve for molecular mass determination was obtained using the LMW gel filtration calibration kit from Sigma-Aldrich.

RESULTS AND DISCUSSION

Production of Mature Forms of TgFNR and TgFd. Recently, the actual N-terminus of mature TgFNR was experimentally determined to be residue Ala143 of its precursor protein (*24*). In previous studies (*9*, *14*), in the absence of such information, we characterized presumed "mature" TgFNRs that were either shorter or longer than the authentic enzyme, starting at residue Ser150 or Leu121, respectively. In the work presented here, all experiments were carried out on a TgFNR form possessing the correct N-terminus. Similarly, protein−protein interactions were here studied using a recombinant mature form of TgFd lacking any His tag extension. The recombinant purified proteins used in this study contained the respective prosthetic group, i.e., FAD or [2Fe-2S], in a 1:1 ratio with the apoprotein, based on spectral analysis.

Limited Proteolysis of TgFNR. The proteolytic degradation of TgFNR in the absence of ligands, produced by proteases of different specificity, was analyzed by SDS−PAGE. As shown in Figures 2−4, trypsin, Glu-C endoproteinase, Asp-N endoproteinase, and thermolysin generated a discrete number

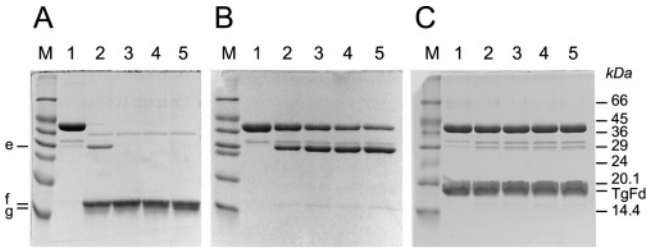

FIGURE 3: SDS−PAGE patterns of degradation of TgFNR by thermolysin in the absence and presence of $NADP^+$ or TgFd. Lane M contained molecular mass markers. Lane 1 contained mixtures before thermolysin addition. Lanes 2−5 contained mixtures after incubation for 1, 5, 15, and 40 min, respectively. Thermolysin was present in a mass ratio relative to TgFNR as specified below. (A) Incubation with 10% thermolysin in the absence of TgFNR ligands. (B) Incubation with 1% thermolysin in the absence of TgFNR ligands. (C) Incubation with 1% thermolysin in the presence of TgFd at a saturating concentration.

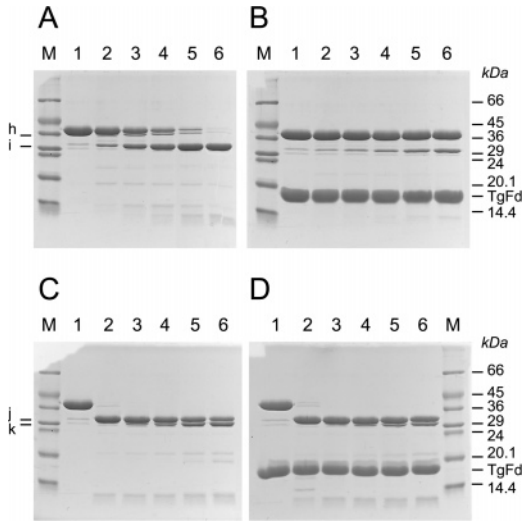

FIGURE 4: SDS−PAGE patterns of degradation of TgFNR by Glu-C and Asp-N endoproteinases in the absence and presence of TgFd. Lane M contained molecular mass markers. Lane 1 contained mixtures before protease addition. Lanes 2−6 contained mixtures after incubation for 1, 5, 10, 20, and 40 min, respectively, with Glu-C or Asp-N protease in mass ratios of 1 or 1.25% relative to TgFNR. (A) Incubation of TgFNR with Glu-C in the absence of ligands. (B) Incubation with Glu-C in the presence of TgFd at a saturating concentration. (C) Incubation of TgFNR with Asp-N in the absence of ligands. (D) Incubation with Asp-N in the presence of TgFd at a saturating concentration.

of polypeptides following a similar fragmentation pattern: the mature TgFNR of apparently 41 kDa was very quickly degraded to polypeptides with molecular masses between 21 and 37 kDa (bands a−c, e, and h−k), which were then converted to shorter species in the 15−18 kDa range (bands d, f, and g) at a much slower rate. Instead, chymotrypsin hydrolyzed so many peptide bonds in TgFNR that a definite proteolysis pattern could not be recognized and its action was thus not further investigated. The effect of the presence of TgFNR substrates during limited proteolysis was then analyzed by including saturating concentrations of either $NADP^+$ or TgFd in the reaction mixtures. Binding of TgFd to TgFNR clearly protected several of the sites whose cleavage by trypsin (Figure 2C,D), thermolysin (Figure 3B,C), or Glu-C endoproteinase (Figure 4A,B) yielded polypeptides in the 29−37 kDa range. The presence of TgFd also resulted in a slightly but significantly slower rate of

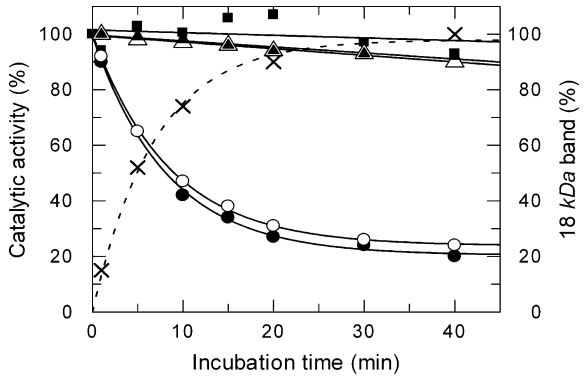

FIGURE 5: Effect of limited proteolysis by different proteases on the catalytic activities of TgFNR. Time courses of the catalytic activities of TgFNR during the incubation with 1% thermolysin (■), 10% trypsin (● and ○), or 10% trypsin in the presence of $NADP^+$ (▲ and △). Filled symbols represent data for the NADPH-$K_3Fe(CN)_6$ reductase activity and empty symbols data for the TgFd-dependent NADPH-cytochrome *c* reductase activity of the limited proteolysis mixtures. Times signs represent the relative intensity of the 18 kDa band (band d) in the SDS−PAGE gel of Figure 2A.

conversion of band j to k during Asp-N treatment of TgFNR (Figure 4C,D). In contrast, $NADP^+$ prevented only the appearance of the 18 kDa band produced by trypsin (Figure 2A,B, band d).

Although all the proteases described effectively cut the polypeptide chain of TgFNR at multiple sites, only the treatment with trypsin resulted in a significant loss of catalytic activity (Figure 5). The TgFd-dependent cytochrome *c* reductase activity and the ferricyanide reductase activity of the flavoenzyme were lost approximately at the same rate. The activity decay matched the kinetics of the formation of the 18 kDa band observed via SDS−PAGE. The presence of $NADP^+$ during trypsin treatment, which, as already mentioned, prevented the formation of the 18 kDa species, protected the enzyme against inactivation (Figure 5). The similar kinetics of enzyme inactivation, regardless of the electron acceptor used in the assay (either ferricyanide or TgFd), as well as the protection by $NADP^+$ indicate that it is the interaction between the enzyme and NADPH that is affected by trypsin treatment. It is conceivable that most of the polypeptides of TgFNR remained associated after cleavage by the various proteases, preserving the conformation of the enzyme, since the fully proteolyzed enzyme maintained a significant fraction of its catalytic activity. Indeed, due to the expected compactness of the conserved part of the TgFNR fold (*13*), dissociation of large polypeptides containing secondary structure elements would likely result in the collapse of the whole protein molecule and in its complete inactivation.

To map the peptide bonds cleaved by the various proteases in the TgFNR sequence, the protein fragments separated by SDS−PAGE were N-terminally sequenced. In general, the proteolysis products were identified by combining the result of sequencing with their apparent molecular mass in SDS−PAGE, as shown in Table 1. Since in the case of trypsin fragmentation the large number of peptides made their identification difficult, the hypothesized sequence was confirmed by the mass information provided by MALDI-TOF analysis of the proteolysis mixtures (Table 1). We identified in TgFNR a total of 11 peptide bonds susceptible to proteolysis, clustered within four well-defined stretches

Table 1: Identification of the Proteolytic Products Generated by Limited Proteolysis of TgFNR

protease	band in SDS−PAGE[a]	apparent molecular mass (SDS−PAGE) (kDa)	*m/z* by mass spectrometry (kDa)	N-terminal sequence[b]	putative fragment[c]	calculated molecular mass[d] (kDa)
trypsin	a	34	nd[e]	NSVQPDGQG	Asn97−Tyr355	28.61
	b	30	nd[e]	RLLPRIYSIASS	Arg118−Tyr355	26.41
	c	21.4	20.19	NSVQPDGQGQQ	Asn97−Lys284	20.20
			19.78		Asn97−Lys279	19.76
	d	18	18.04	RLLPRIYSIA	Arg118−Lys284	18.01
			17.54		Arg118−Lys279	17.56
	nd[e]	10	10.50	VAVNTFPASPLI	Val18−Arg117	10.50
	nd[e]	8	8.90	NPQGKKLYI	Asn280−Tyr355	8.91
			8.38	KLYIQDVV	Lys285−Tyr355	8.38
			8.30	VAVNTFRPA	Val18−Arg96	8.30
thermolysin	e	29.3		I(C)KRRLLPRIYSI	Ile114−Tyr355	26.0
	f	15.7		AAQPANRPKVLL	Ala229−Tyr355	14.7
	g	15.4		I(C)KRRLLPRIYS	Ile114−Ser228	12.2
Glu-C	h	37		LRVAVN	Leu16−Tyr355	37.2
	i	30		STSQR	Ser92−Tyr355	29.2
Asp-N	j	33		DESTSQR	Asp90−Tyr355	29.4
	k	28.7		DGQGQQP	Asp102−Tyr355	28

[a] The letters identify the bands observed in the analytical SDS−PAGE gels of Figures 2−4. Bands corresponding to polypeptides with a molecular mass lower than 12 kDa were not visible in analytical gels. [b] Cysteine residues are inferred since the sequencing procedure did not allow their direct identification; all peptides were sequenced for a number of residues sufficient for the unambiguous identification of their N-termini. [c] C-Terminal residues of the peptides are inferred on the basis of their molecular mass and the N-termini of other fragments. [d] For the peptides generated by trypsin, the monoisotopic molecular mass values are reported to allow comparison with mass spectrometry data. [e] Not detected.

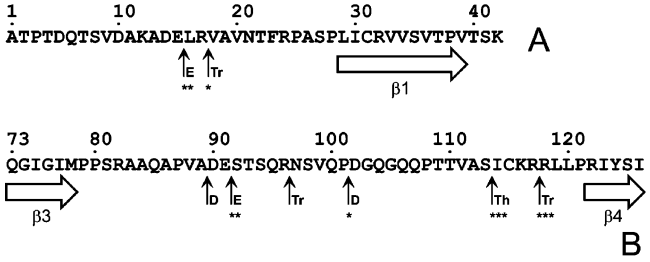

FIGURE 6: Sequence of polypeptide regions of TgFNR involved in TgFd binding identified by ligand protection against limited proteolysis. The primary structure of relevant regions of TgFNR is shown with residues numbered according to the sequence of the mature enzyme. Secondary structure elements are shown as in Figure 1. Vertical arrows indicate protease-sensitive peptide bonds. Asterisks rank the protective effect of binding of TgFd on cleavable sites as poor (one), medium (two), or strong (three). Proteases are symbolized as follows: Tr, trypsin; Th, thermolysin; E, Glu-C; D, Asp-N. (A) N-Terminal region and (B) region encompassing insertion II.

of its amino acid sequence: the N-terminal region, the 81−118 subdomain, the 225−231 insert, and the 276−288 region. Two sites were localized in the N-terminal region of TgFNR: the peptide bonds at the carboxy side of Glu15 and Arg17 (Figure 6A). The N-terminal residues are not conserved among distantly related plant-type FNRs, the sequence similarity starting only at residue 20 (mature TgFNR numbering). The sensitivity to proteases of the 1−19 segment of TgFNR was expected. Indeed, the N-terminal regions of spinach leaf and maize root FNRs were cleaved by various proteases in limited proteolysis experiments (*25*, *26*). The solvent accessibility and flexibility of the nonconserved N-terminal polypeptide of various plant FNRs have been indicated by different techniques. Most of this region was found disordered in spinach leaf FNR by X-ray crystallography (*27*), and it was shown to be highly flexible and protruding into the solvent as a fluctuating tail in maize leaf FNR by NMR spectroscopy (*21*) and X-ray scattering analysis (*28*), respectively. While we could not obtain any information about the effect of TgFd binding on the cleavage by trypsin at Arg17, such protection was evident in the case of the action of the Glu-C protease at Glu15 (Figure 4A,B, band h). Thus, it seems that the N-terminal polypeptide of TgFNR participates in the interaction with TgFd. Very interestingly, more than half of the mapped cleavage sites are clustered in the 89−118 polypeptide region of TgFNR, within the species-specific subdomain of the enzyme that contains insertion II and connects β strands 3 and 4 of the FAD-binding β barrel (see Figure 1). This region includes the most protease-sensitive peptide bonds of TgFNR, such as those at the carboxy side of Arg96 and Glu91, cleaved by trypsin and Glu-C protease, respectively, and those at the amino side of Ile114 and Asp90, cleaved by thermolysin and Asp-N protease, respectively. The very high susceptibility of this region to protease attack is also demonstrated by the fact that purified recombinant TgFNR preparations always exhibited a minor 30 kDa band in SDS−PAGE gels that can be attributed to a species probably arising by a cleavage around residue 90. The primary structure of this region, with the proteolysis sites and a map of the TgFd protection pattern, is detailed in Figure 6B. These results indicate that the species-specific TgFNR subdomain is solvent-exposed and possesses a high segmental mobility. Furthermore, it is remarkable that the cleavage of most of the sites located within this proteolysis hot spot are protected by TgFd binding. TgFd strongly protected against the cleavage of two peptide bonds in the C-terminal part of the polypeptide (Ser113-Ile114 and Arg117-Arg118), where a highly positively charged sequence (KRR) is present. On the other hand, for two cleavage sites in the N-terminal part of the polypeptide (Ala89-Asp90 and Arg96-Asn97), no protection was observed, while the remaining sites exhibited an intermediate behavior. Specific subregions of the 81−118 polypeptide of TgFNR might therefore participate in formation of a complex with TgFd. In non apicomplexan FNRs, the 81−118 subdomain of TgFNR is replaced with a much shorter (10 residues in spinach leaf FNR) solvent-exposed loop, which is certainly much more rigid: it has an ordered conformation

in all FNR crystal structures known (*29*), and although it is protease-sensitive in the maize root FNR (*26*), it is resistant in the spinach leaf enzyme (*25*). This loop has been shown in the FNRs from various sources to be involved in Fd binding by several different approaches (*21*, *25*, *30*, *31*). Despite its increased length and the lack of any sequence similarity, the 81−118 region of TgFNR seems to have maintained such a functional role in protein−protein interaction.

The peptide bond between Ser228 and Ala229 was cleaved by thermolysin, indicating that another *T. gondii*-specific region of TgFNR, the 225−231 insertion, is flexible and solvent-exposed. The absence of protection by ligands is in agreement with the expected localization of this region on the opposite side of the molecule with respect to the NADP(H) and TgFd binding sites. Finally, cleavage by trypsin of the two peptide bonds on the carboxy side of Lys279 and Lys284 was responsible for the formation of the 18 and 8 kDa bands observed in SDS−PAGE and for the partial inactivation of the enzyme. Proteolysis at these positions was strongly protected by $NADP^+$. This region, which has a highly conserved sequence in all plant-type FNRs, was previously shown in higher-plant FNRs to be sensitive to proteases and to be protected by $NADP^+$ (*25*, *26*). In all FNRs of known three-dimensional structure, this peptide segment forms a surface loop at the N-terminal side of the Rossmann fold motif of the NADP(H)-binding domain, making contacts with the 2′-phosphoadenosyl moiety of the bound dinucleotide (*27*). Thus, limited proteolysis data confirmed for the homologous region of TgFNR a similar structure and function in NADP(H) binding.

By sequence alignment, the 51−58 segment (insertion I) appears to be inserted in a sequence position that in FNRs of known three-dimensional structure corresponds to the middle of β strand 2 of the antiparallel barrel that binds FAD (Figure 1). The insert is thus expected to alter part of the β strand and to form a bulge protruding from the barrel. The resistance of this polypeptide segment to proteases, despite the presence of potential Glu-C and thermolysin sites, indicates that either it is somehow buried within the molecule interior or it is exposed but adopts a rigid conformation, although it is not obvious how it is accommodated within the rest of the structure.

Structure and Function of the 81−118 Subdomain of TgFNR As Studied by Protein Engineering. Results from limited proteolysis pointed to the involvement of the species-specific subdomain of TgFNR in the binding of the protein substrate TgFd. To further investigate the properties of this peptide segment, an engineered form of the enzyme, where this sequence was entirely deleted by site-directed mutagenesis, was produced. To optimize the design of the mutant, the conformation of the loop that in plant FNRs connects β strands 3 and 4 of the β barrel of the FAD-binding domain was examined. The two or three terminal residues on both sides of this loop make contacts with the surrounding residues from the nearby parts of the molecule and might thus be important for the overall stability of the protein. For this reason, when the TgFNR mutant was designed, the sequence up to Pro80 and starting from Leu119 was maintained. The two ends of the polypeptide chain were joined by a highly flexible Gly tripeptide to prevent possible structural strains within the barrel motif. The engineered protein was termed

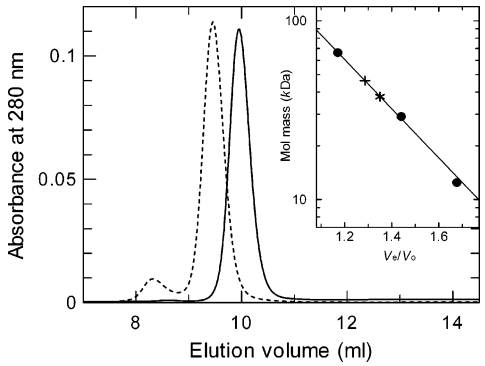

FIGURE 7: Analytical gel filtration of wild-type and mutant TgFNR forms. Wild-type TgFNR (- - -) and TgFNRΔ(81−118)G_3 (—) were individually chromatographed on a Superdex 75 HR 10/30 column at a flow rate of 0.5 mL/min at room temperature. The inset shows the calibration curve obtained by running a set of molecular mass standards (●): cytochrome *c* (12.4 kDa), carbonic anhydrase (29 kDa), and bovine serum albumin (66 kDa). The apparent molecular masses of wild-type (+) and mutant TgFNR (∗) were determined according to this curve.

Table 2: Kinetic Parameters of TgFNRΔ(81−118)G_3 in Comparison to Those of the Wild-Type Enzyme

	NADPH-INT reductase reaction[a]		
enzyme form	k_{cat}[c]	K_m^{NADPH} (μM)	k_{cat}/K_m^{NADPH} ($s^{-1}\,\mu M^{-1}$)
TgFNRΔ(81−118)G_3	540 ± 30	15 ± 1	36 ± 3
TgFNR	424 ± 25	16 ± 1	27 ± 3

	NADPH-cytochrome *c* reductase (TgFd-dependent) reaction[b]		
enzyme form	k_{cat}[c]	K_m^{TgFd} (μM)	k_{cat}/K_m^{TgFd} ($s^{-1}\,\mu M^{-1}$)
TgFNRΔ(81−118)G_3	260 ± 8	18 ± 2	14 ± 1
TgFNR	130 ± 3	2.8 ± 0.2	48 ± 4

[a] Activity was assayed at 25 °C in 200 mM Tris-HCl (pH 9.0) containing 70 mM NaCl and 0.1% Triton X-100. [b] Activity was assayed at 25 °C in 100 mM Tris-HCl (pH 8.2) using 40 μM cytochrome *c*. [c] Rate values are expressed in electron equivalents per second.

TgFNRΔ(81−118)G_3. It was overproduced in *E. coli* at an expression level comparable to that of the wild-type protein and successfully purified using the same procedure. The purified mutant protein contained FAD in a 1:1 ratio with respect to the apoprotein and displayed absorption and fluorescence properties very similar to those of the wild-type protein (Figures 1 and 2 of the Supporting Information). Thus, the deletion did not appear to affect the folding or stability of the enzyme. By gel filtration, the mutant form displayed a molecular mass of 37.6 kDa, close to the calculated value of 35 kDa (Figure 7). The same technique gave for the wild-type TgFNR an apparent mass of 46.3 kDa, which exceeded by more than 8.7 kDa the calculated value of 39 kDa. Thus, the deleted peptide contributes to the hydrodynamic properties of TgFNR to an extent much higher than expected on the basis of its mass (4026 Da), suggesting that the species-specific subdomain of TgFNR is a structure that severely protrudes from the core of the molecule.

The catalytic properties of wild-type and mutant TgFNRs were compared by performing steady-state kinetic analyses of both the diaphorase and cytochrome *c* reductase reactions. The relevant kinetic parameters are listed in Table 2. The deletion did not affect the K_m for NADPH. Rather, it

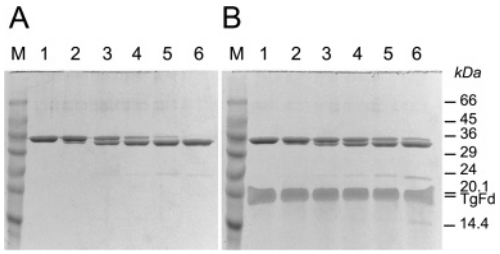

FIGURE 8: SDS−PAGE analysis of the time course of trypsin cleavage within the N-terminal region of TgFNRΔ(81−118)G_3 in the absence and presence of TgFd. Lane M contained molecular mass markers. Lane 1 contained mixtures before trypsin addition. Lanes 2−6 contained mixtures after incubation with 1% trypsin for 1, 5, 10, 20, and 40 min, respectively. To simplify the interpretation of the results, proteolysis was carried out in the presence of NADP$^+$, which prevents proteolysis in the C-terminal domain. (A) Incubation of TgFNRΔ(81−118)G_3 in the absence of TgFd. (B) Incubation of TgFNRΔ(81−118)G_3 in the presence of TgFd.

moderately increased the k_{cat} of the reduction of both electron acceptors and, more interestingly, increased the K_m for TgFd by a factor of 7. TgFNRΔ(81−118)G_3 was significantly more resistant to limited proteolysis than the wild-type protein. Predictably, the deletion removed the six protease-sensitive sites located in the 81−118 subdomain (see Figure 6B), however without exposing new regions amenable to proteolysis. All the other cleavage sites observed in the wild-type protein were still accessible in TgFNRΔ(81−118)G_3. This lower number of cleavage sites in the mutant protein gave us the opportunity to better analyze the proteolysis in the N-terminal peptide of TgFNR. As shown in Figure 8, in addition to the Glu15-Leu16 site (see Figure 3A,B), TgFd can protect the Arg17-Val18 peptide bond. Following cleavage with Glu-C endoproteinase at Glu15, TgFNRΔ-(81−118)G_3 was eluted from the gel filtration column with a retention volume of 10.36 mL (not shown), which is higher by 0.4 ± 0.01 mL as compared to that of the intact TgFNRΔ-(81−118)G_3 mutant (see Figure 7). The strong effect of proteolysis in the N-terminal region on the apparent molecular mass of the enzyme indicates that, unlike larger peptides that remain associated after cleavage, the highly flexible 1−15 polypeptide dissociates from the rest of the protein as the Glu15-Leu16 bond is hydrolyzed. Similarly, proteolysis by trypsin at Arg17 is expected to generate a corresponding truncated form.

To ascertain whether the increased K_m of TgFNRΔ(81−118)G_3 for TgFd reflected a decreased affinity for the protein substrate, the two TgFNR forms were analyzed by affinity chromatography on a column of immobilized TgFd. Figure 9A clearly shows that the retention volume of the deletion mutant was significantly lower than that of wild-type TgFNR. Such an effect (20% difference in retention) can be attributed to a 10-fold increase in K_d, based on the behavior of single-point mutants of FNR on the same affinity column (*14*). To evaluate the actual role of the N-terminal peptide of TgFNR in TgFd binding, TgFNRΔ(81−118)G_3 forms, which have been N-terminally truncated by treatment with trypsin or Glu-C endoproteinase, were analyzed by affinity chromatography, as shown in Figure 9B. Quite surprisingly, the removal of the first 15 or 17 residues of the enzyme resulted in an increased retention on the affinity column, reflecting a higher affinity for TgFd compared to that of the parent protein. This indicates that the N-terminal peptide of TgFNR

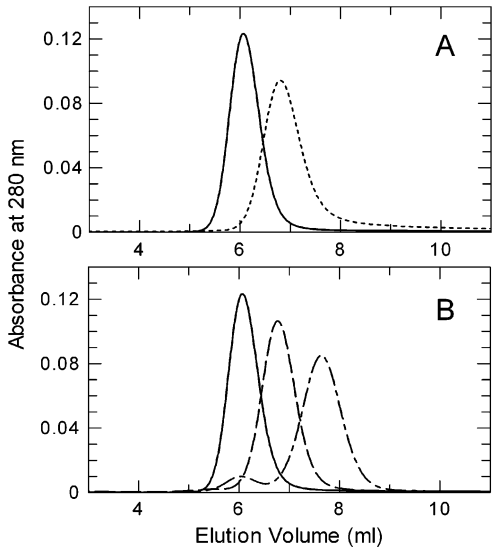

FIGURE 9: Effects of the deletion of the *T. gondii*-specific subdomain and of the proteolysis in its N-terminal region on the affinity of TgFNR for TgFd, as determined by affinity chromatography. The chromatograms were obtained at room temperature by loading ca. 250 μg of each TgFNR form on a column packed with 1 mL of TgFd-conjugated resin. Elution was accomplished with a gradient from 0 to 1 M NaCl in 10 column volumes at a flow rate of 0.5 mL/min: (A) wild-type TgFNR (- - -) and TgFNRΔ(81−118)G_3 (—) and (B) TgFNRΔ(81−118)G_3 (—), TgFNRΔ(81−118)-G_3 treated with 1% trypsin for 40 min in the presence of NADP$^+$ (— — —), and TgFNRΔ(81−118)G_3 treated with Glu-C endoproteinase for 40 min (— - —).

makes repulsive interprotein contacts within the TgFNR−TgFd complex. This conclusion is in contrast with the recent observation that the N-terminal region of corn leaf FNR participates in Fd binding (*21*), suggesting diverse roles for this poorly conserved polypeptide region in FNRs from different species. On the other hand, the opposite roles of the N-terminal segment of plant leaf and *T. gondii* FNRs in the interaction with Fd fit well with their acid−base character. In leaf FNRs, this polypeptide is rich in positively charged residues, whereas in TgFNR, it contains mostly negatively charged ones. In this context, the large differential effect on TgFd affinity of cleaving the N-terminal region of TgFNR at sites that are just two peptide bonds apart is remarkable. The strong difference between Glu-C endoproteinase and trypsin in increasing the stability of the TgFNRΔ-(81−118)G_3−TgFd complex can be interpreted on the basis of the fact that Glu-C cleavage maintains the strongly basic Arg17 residue (see Figure 6A). It has been proposed that flexible binding sites could increase the available search space in the processes of protein−protein recognition (*32*). Maeda and co-workers argued that the flexible N-terminal region of maize leaf FNR might have such a "bait" role with respect to Fd in the initial steps of the binding mechanism (*21*). In TgFNR (and perhaps in all apicomplexan FNRs), this function seems to have been lost by the N-terminal peptide and transferred to the 81−118 subdomain. The proximity of both regions to the protein substrate in the TgFNR−TgFd complex is in agreement with the homology model previously described (*14*), as shown in Figure 10A. According to this model, most of the peptide bonds of TgFNR found protected by TgFd binding are located within the interaction surface or in its immediate surroundings (Figure 10B).

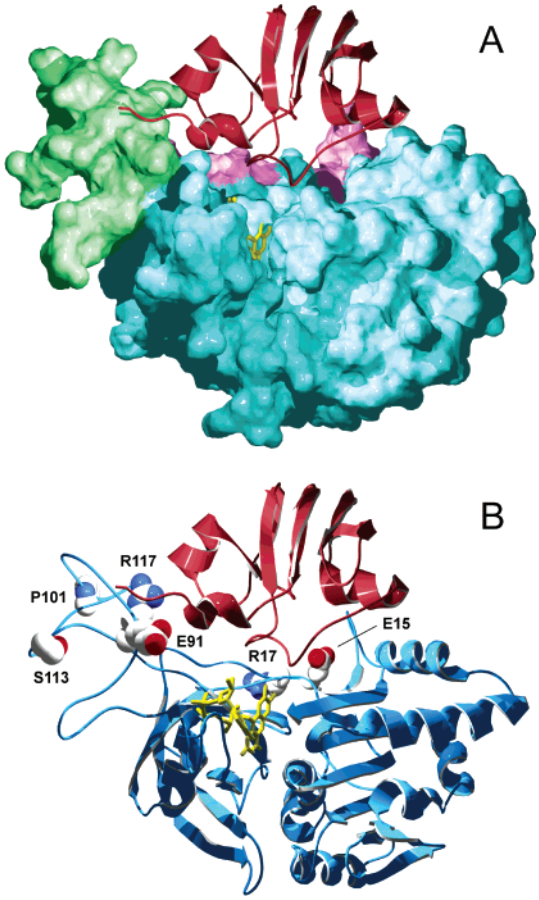

FIGURE 10: Localization in the three-dimensional structure of the TgFNR of the polypeptide regions identified as being involved in TgFd binding. Homology model of the TgFNR−TgFd complex (*14*). The ribbon model of TgFd is colored red; its [2Fe-2S] cluster has been omitted for clarity. (A) Molecular surface of TgFNR. The 81−118 subdomain and the N-terminal peptide are colored green and magenta, respectively. The rest of the molecule is colored blue. (B) The ribbon diagram of TgFNR is colored blue. FAD is represented as a yellow wireframe. The side chains of the residues at the amino side of the peptide bonds whose hydrolysis was protected by TgFd are shown in space-filling representation. The model has been drawn using Swiss-PDBViewer version 3.7 (http://www.expasy.org/spdbv) and POV-Ray version 3.6 (Persistence of Vision Raytracer Pty. Ltd.).

CONCLUSIONS

The results reported here allow us to conclude that two of the three characteristic insertions of TgFNR are solvent-exposed and structurally flexible. The largest of them (insertion II) is suggested to give rise to a 38-residue intrinsically unstructured subdomain, protruding from the top of the FAD-binding β barrel. Such a species-specific subdomain does not have major functions in protein folding and stability. Rather, it participates in TgFd binding, significantly increasing the stability of the protein−protein complex and improving the catalytic efficiency of the enzyme in the electron transfer to TgFd. On the other hand, the 20−25 N-terminal residues of the polypeptide chain, which in plant leaf FNRs has been shown to stabilize the FNR−Fd complex, do not have this role in TgFNR. The findings of this study represent a significant contribution to the identification of the TgFd-binding region of TgFNR and allowed the identification of a specific polypeptide segment involved in protein−protein interaction. This information is of value for the design of peptides or peptidomimetic compounds acting as dissociators of the TgFNR−TgFd complex. If they are found to be effective, such compounds could represent leads in the development of novel drugs against diseases caused by Apicomplexa.

ACKNOWLEDGMENT

We thank P. Andrew Karplus for performing a comparative analysis of the structure of the loop that in plant FNRs replaces the TgFNR subdomain. We are grateful to Paul M. Selzer for providing us the atom coordinates of the TgFNR−TgFd complex model.

SUPPORTING INFORMATION AVAILABLE

Two figures reporting the absorption and fluorescence emission spectra of TgFNR and TgFNRΔ(81−118)G_3. This material is available free of charge via the Internet at http://pubs.acs.org.

REFERENCES

1. Wilson, R. J. (2002) Progress with parasite plastids, *J. Mol. Biol. 319*, 257−274.
2. Foth, B. J., and McFadden, G. I. (2003) The apicoplast: A plastid in *Plasmodium falciparum* and other Apicomplexan parasites, *Int. Rev. Cytol. 224*, 57−110.
3. Abrahamsen, M. S., Templeton, T. J., Enomoto, S., Abrahante, J. E., Zhu, G., Lancio, C. A., Deng, M., Liu, C., Widmer, G., Tzipori, S., Buck, G. A., Xu, P., Bankier, A. T., Dear, P. H., Konfortov, B. A., Spriggs, H. F., Iyer, L., Anantharaman, V., Aravind, L., and Kapur, V. (2004) Complete genome sequence of the apicomplexan, *Cryptosporidium parvum*, *Science 304*, 441−445.
4. Fast, N. M., Kissinger, J. C., Roos, D. S., and Keeling, P. J. (2001) Nuclear-encoded, plastid-targeted genes suggest a single common origin for apicomplexan and dinoflagellate plastids. *Mol. Biol. Evol. 18*, 418−426.
5. Fichera, M. E., and Roos, D. S. (1997) A plastid organelle as a drug target in apicomplexan parasites, *Nature 390*, 407−409.
6. Seeber, F. (2003) Biosynthetic pathways of plastid-derived organelles as potential drug targets against parasitic apicomplexa, *Curr. Drug Targets: Immune, Endocr. Metab. Disord. 3*, 99−109.
7. Ralph, S. A., D'Ombrain, M. C., and McFadden, G. I. (2001) The apicoplast as an antimalarial drug target, *Drug Resist. Updates 4*, 145−151.
8. Vollmer, M., Thomsen, N., Wiek, S., and Seeber, F. (2001) Apicomplexan parasites possess distinct nuclear encoded but apicoplast-localized plant-type ferredoxin-$NADP^+$-reductase and ferredoxin, *J. Biol. Chem. 276*, 5483−5490.
9. Pandini, V., Caprini, G., Thomsen, N., Aliverti, A., Seeber, F., and Zanetti, G. (2002) Ferredoxin-$NADP^+$ reductase and ferredoxin of the protozoan parasite *Toxoplasma gondii* interact productively in vitro and in vivo, *J. Biol. Chem. 277*, 48463−48471.
10. Röhrich, R. C., Troschke, K., Englert, N., Reichenberg, A., Hintz, M., Seeber, F., Balconi, E., Aliverti, A., Zanetti, G., Köhler, U., Pfeiffer, M., Beck, E., Jomaa, H., and Wiesner, J. (2005) Reconstitution of an apicoplast-localised electron-transfer pathway involved in the isoprenoid biosynthesis of *Plasmodium falciparum*, *FEBS Lett. 579*, 6433−6438.
11. Jomaa, H., Wiesner, J., Sanderbrand, S., Altincicek, B., Weidemeyer, C., Hintz, M., Turbachova, I., Eberl, M., Zeidler, J., Lichtenthaler, H. K., Soldati, D., and Beck, E. (1999) Inhibitors of the nonmevalonate pathway of isoprenoid biosynthesis as antimalarial drugs, *Science 285*, 1573−1576.
12. Seeber, F., Aliverti, A., and Zanetti, G. (2005) The plant-type ferredoxin-$NADP^+$ reductase/ferredoxin redox system as a possible drug target against apicomplexan human parasites, *Curr. Pharm. Des. 11*, 3159−3172.
13. Bednarek, A., Wiek, S., Lingelbach, K., and Seeber, F. (2003) *Toxoplasma gondii*: Analysis of the active site insertion of its ferredoxin-$NADP^+$-reductase by peptide-specific antibodies and homology-based modelling, *Exp. Parasitol. 103*, 68−77.

14. Thomsen-Zieger, N., Pandini, V., Caprini, G., Aliverti, A., Cramer, J., Selzer, P. M., Zanetti, G., and Seeber, F. (2004) A single in vivo-selected point mutation in the active center of *Toxoplasma gondii* ferredoxin-NADP$^+$ reductase leads to an inactive enzyme with greatly enhanced affinity for ferredoxin, *FEBS Lett. 576*, 375−380.
15. Hoffman, S. L., Subramanian, G. M., Collins, F. H., and Venter, J. C. (2002) *Plasmodium*, human and *Anopheles* genomics and malaria, *Nature 415*, 702−709.
16. Clarke, J. L., Sodeinde, O., and Mason, P. J. (2003) A unique insertion in *Plasmodium berghei* glucose-6-phosphate dehydrogenase-6-phosphogluconolactonase: Evolutionary and functional studies, *Mol. Biochem. Parasitol. 127*, 1−8.
17. Sarma, G. N., Savvides, S. N., Becker, K., Schirmer, M., Schirmer, R. H., and Karplus, P. A. (2003) Glutathione reductase of the malarial parasite *Plasmodium falciparum*: Crystal structure and inhibitor development, *J. Mol. Biol. 328*, 893−907.
18. Birkholtz, L.-M., Wrenger, C., Joubert, F., Wells, G. A., Walter, R. D., and Louw, A. I. (2004) Parasite-specific inserts in the bifunctional S-adenosylmethionine decarboxylase/ornithine decarboxylase of *Plasmodium falciparum* modulate catalytic activities and domain interactions, *Biochem. J. 377*, 439−448.
19. Morales, R., Charon, M.-H., Kachalova, G., Serre, L., Medina, M., Gómez-Moreno, C., and Frey, M. (2000) A redox-dependent interaction between two electron-transfer partners involved in photosynthesis, *EMBO Rep. 1*, 271−276.
20. Kurisu, G., Kusunoki, M., Katoh, E., Yamazaki, T., Teshima, K., Onda, Y., Kimata-Ariga, Y., and Hase, T. (2001) Structure of the electron-transfer complex between ferredoxin and ferredoxin-NADP$^+$ reductase, *Nat. Struct. Biol. 8*, 117−121.
21. Maeda, M., Lee, Y. H., Ikegami, T., Tamura, K., Hoshino, M., Yamazaki, T., Nakayama, M., Hase, T., and Goto, Y. (2005) Identification of the N- and C-terminal substrate binding segments of ferredoxin-NADP$^+$ reductase by NMR, *Biochemistry 44*, 10644−10653.
22. Piubelli, L., Aliverti, A., Bellintani, F., and Zanetti, G. (1995) Spinach ferredoxin I: Overproduction in *Escherichia coli* and purification, *Protein Expression Purif. 6*, 298−304.
23. Aliverti, A., Piubelli, L., Zanetti, G., Lübberstedt, T., Herrmann, R. G., and Curti, B. (1993) The role of cysteine residues of spinach ferredoxin-NADP$^+$ reductase as assessed by site-directed mutagenesis, *Biochemistry 32*, 6374−6380.
24. Harb, O. S., Chatterjee, B., Fraunholz, M. J., Crawford, M. J., Nishi, M., and Roos, D. S. (2004) Multiple functionally redundant signals mediate targeting to the apicoplast in the apicomplexan parasite *Toxoplasma gondii*, *Eukaryotic Cell 3*, 663−674.
25. Gadda, G., Aliverti, A., Ronchi, S., and Zanetti, G. (1990) Structure−function relationship in spinach ferredoxin-NADP$^+$ reductase as studied by limited proteolysis, *J. Biol. Chem. 265*, 11955−11959.
26. Aliverti, A., Faber, R., Finnerty, C. M., Ferioli, C., Pandini, V., Negri, A., Karplus, P. A., and Zanetti, G. (2001) Biochemical and crystallographic characterization of ferredoxin-NADP$^+$ reductase from nonphotosynthetic tissues, *Biochemistry 40*, 14501−14508.
27. Karplus, P. A., Daniels, M. J., and Herriott, J. R. (1991) Atomic structure of ferredoxin-NADP$^+$ reductase: Prototype for a structurally novel flavoenzyme family, *Science 251*, 60−66.
28. Maeda, M., Hamada, D., Hoshino, M., Onda, Y., Hase, T., and Goto, Y. (2002) Partially folded structure of flavin adenine dinucleotide-depleted ferredoxin-NADP$^+$ reductase with residual NADP$^+$ binding domain, *J. Biol. Chem. 277*, 17101−17107.
29. Karplus, P. A., and Faber, H. R. (2004) Structural aspects of plant ferredoxin:NADP$^+$ oxidoreductases, *Photosynth. Res. 81*, 303−315.
30. Aliverti, A., Jansen, T., Zanetti, G., Ronchi, S., Herrmann, R. G., and Curti, B. (1990) Expression in *Escherichia coli* of ferredoxin: NADP$^+$ reductase from spinach. Bacterial synthesis of the holoflavoprotein and of an active enzyme form lacking the first 28 amino acid residues of the sequence, *Eur. J. Biochem. 191*, 551−555.
31. Aliverti, A., Corrado, M. E., and Zanetti, G. (1994) Involvement of lysine-88 of spinach ferredoxin-NADP$^+$ reductase in the interaction with ferredoxin, *FEBS Lett. 343*, 247−250.
32. Shoemaker, B. A., Portman, J. J., and Wolynes, P. G. (2000) Speeding molecular recognition by using the folding funnel: The fly-casting mechanism, *Proc. Natl. Acad. Sci. U.S.A. 97*, 8868−8873.

BI052326W